Independent component analysis for unmixing multi-wavelength photoacoustic images

Lu An and Ben Cox

Department of Medical Physics and Biomedical Engineering, University College London, Gower Street, WC1E 6BT, UK

ABSTRACT

Independent component analysis (ICA) is a blind source unmixing method that may be used under certain circumstances to decompose multi-wavelength photoacoustic (PA) images into separate components representing individual chromophores. It has the advantages of being fast, easy to implement and computationally inexpensive. This study uses simulated multi-wavelength PA images to investigate the conditions required for ICA to be an accurate unmixing method and compares its performance to linear inversion. An approximate fluence adjustment based on spatially homogeneous optical properties equal to that of the background region was applied to the PA images before unmixing with ICA or LI. ICA is shown to provide accurate separation of the chromophores in cases where the absorption coefficients are lower than certain thresholds, some of which are comparable to physiologically relevant values. However, the results also show that the errors associated with ICA abruptly increase when the absorption is increased beyond these thresholds, due to the inability to identify the relevant chromophore components. In addition, the accuracy of ICA decreases in the presence of spatially inhomogeneous absorption in the background.

Keywords: spectral unmixing, ICA, linear inversion, photoacoustic imaging, quantitative photoacoustic tomography, fluence correction, blind source separation

1. INTRODUCTION

The ability to clearly separate the endogenous chromophores or exogenous biomarkers from the background tissue and to accurately estimate their concentrations is crucial to many preclinical and clinical applications of PA imaging. However, the PA image is non-linearly related to the chromophore concentrations because the PA signal is a product of both the optical absorption coefficient and the spatially and spectrally varying fluence, which makes spectral unmixing more challenging.

In order to unmix the chromophore components, many *in vivo* multi-wavelength PA imaging studies have used the linear inversion (LI) method, in which the fluence is assumed to be constant, estimated using additional measurements, or approximated based on spatially homogeneous optical properties. Unmixing using LI has the advantages of being fast and simple to implement, but has been shown to have limited accuracy for non-superficial tissue layers.[1]

Independent component analysis (ICA) has been proposed by Glatz *et al*[2] as an alternative technique for unmixing PA images and was shown to provide more accurate results than LI under some circumstances, while maintaining the advantages of ease of implementation and low computational expense. This study investigates the conditions required for ICA to be an accurate unmixing method for quantitative PA imaging and compares its performance to LI using numerically simulated multi-wavelength PA images.

2. INDEPENDENT COMPONENT ANALYSIS

PA images are reconstructions of the initial pressure rise due to the absorption of optical energy. Assuming that the acoustic reconstruction is perfect, a set of PA images with m voxels acquired at n wavelengths, whose contrast originate predominately from k chromophores, can be described using matrix notation as

$$\mathbf{P} = \mathbf{\Phi} \circ (\mathbf{A} (\mathbf{\Gamma} \circ \mathbf{C})) , \tag{1}$$

Photons Plus Ultrasound: Imaging and Sensing 2016, edited by Alexander A. Oraevsky, Lihong V. Wang
Proc. of SPIE Vol. 9708, 970851 · © 2016 SPIE · CCC code: 1605-7422/16/$18 · doi: 10.1117/12.2208137

where $\circ$ denotes the Hadamard product, $\mathbf{P}$ is a $(n \times m)$ matrix with each row corresponding to a reconstruction of the initial pressures at one of the wavelengths, $\mathbf{\Phi}$ is the $(n \times m)$ fluence matrix with each row representing the spatially varying fluence at one of the wavelengths, $\mathbf{A}$ is the $(n \times k)$ mixing matrix with each column representing the wavelength dependent specific absorption coefficient of one of the chromophores, $\mathbf{C}$ is the $(k \times m)$ concentrations matrix with each row representing the concentration distribution of one of the chromophores, and $\mathbf{\Gamma}$ is the $(k \times m)$ matrix with each row representing the spatially varying Grüneisen parameter associated with one of the chromophores. The unmixing methods are not expected to separate $\mathbf{\Gamma}$ from the concentrations because $\mathbf{\Gamma}$ is wavelength independent and scales with the concentrations. It is assumed in this study that $\mathbf{\Gamma}$ is known.

Both ICA and LI are unmixing methods based on a linear model. The initial PA pressure rise is however non-linearly related to the concentrations, due to the spectrally and spatially varying fluence matrix in Eq. 1. An approximation to linearity can be achieved by dividing $\mathbf{P}$ element wise by an approximate estimate of the fluence, $\mathbf{\Phi'}$, such that

$$\frac{\mathbf{P}}{\mathbf{\Phi'}} = \mathbf{P'} \approx \mathbf{A}\left(\mathbf{\Gamma} \circ \mathbf{C}\right). \tag{2}$$

In LI, the mixing matrix with the specific absorption coefficients is assumed to be known. Hence, the chromophore concentrations can be estimated using the pseudoinverse of the mixing matrix, $\mathbf{A}^{\dagger}$:

$$\mathbf{A}^{\dagger}\mathbf{P'} \approx \mathbf{\Gamma} \circ \mathbf{C} \tag{3}$$

Unlike in LI, the mixing matrix is assumed to be unknown in ICA. Instead, ICA aims to decompose the multi-wavelength PA images into the source components, which represent the individual chromophores, based on the assumption that the source components are statistically mutually independent of each other. This is achieved by searching for a mixing matrix, $\mathbf{W}$, that corresponds to the source components, $\mathbf{S}$, whose rows have maximal mutual independence:

$$\mathbf{W}^{\dagger}\mathbf{P'} = \mathbf{S} \tag{4}$$

In the widely used ICA algorithm FastICA,[3] the search is based on the Central Limit Theorem, which states that the probability distribution of the sum of multiple independent variables will always be more Gaussian than the distribution of one of the independent variables alone. The Gaussianity of the probability distribution of the output components is measured using negentropy, which is a normalised version of entropy. Hence, the independent source components are found by iteratively searching for a mixing matrix that maximises the negentropy of each row of $\mathbf{S}$. Provided that the true spatial distributions of the chromophore concentrations are independent, the source components correspond to $\mathbf{S} \approx \mathbf{\Gamma} \circ \mathbf{C}$.

If the fluence was estimated exactly, such that $\mathbf{\Phi'} = \mathbf{\Phi}$, the approximate model in Eq. 2 would be an exact equality and, if the chromophore distributions were independent, both ICA and LI would achieve accurate unmixing of the chromophores. In practice however, $\mathbf{\Phi'}$ is only an approximation of $\mathbf{\Phi}$, and both methods will lead to errors.

3. SIMULATED MULTI-WAVELENGTH PA IMAGES

The two dimensional numerical phantom used in this study has dimensions of 7.36mm x 20.00mm and 20μm spacing between the elements. As indicated in Fig. 1, the phantom has eight circular regions of 0.59mm diameter representing aqueous solutions of copper chloride or nickel chloride in different concentrations. The contrast agents were chosen because they have properties that are desirable for constructing experimental tissue mimicking phantoms. The left column of discs represents copper chloride with concentrations in the ratio of 1:2:3:4, where the uppermost disc has the lowest concentration. The right column of discs contains nickel chloride also with the concentration ratio of 1:2:3:4. Since the specific absorption coefficient of nickel chloride is approximately one order of magnitude lower than that of copper chloride, as shown in Fig. 2(a), the concentrations of nickel chloride are set to be ten times higher than copper chloride to give similar optical absorption. The region outside the

eight discs represents an absorbing and scattering background consisting of India ink and 1% Intralipid diluted in water. The following criteria are satisfied in the numerical phantom:

1. The spatial distributions of the chromophores are independent, so that when the fluence adjustment is perfect, ICA results in accurate unmixing.
2. The specific absorption spectra of the chromophores are such that the mixing matrix **A** is full rank, so that when the fluence adjustment is perfect, LI results in accurate unmixing.

Hence, using this phantom, it is possible to see how inaccuracies in the fluence adjustment affect the accuracy of the unmixing methods.

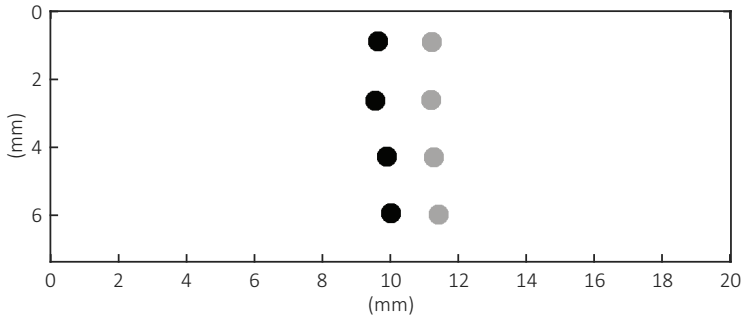

Figure 1. The two dimensional numerical phantom. The black and grey discs represent different concentrations of copper chloride or nickel chloride respectively. The white region represents the absorbing and scattering background solution consisting of India ink, Intralipid and water.

In order to compare the performance of ICA to LI for different levels of absorption, 41 sets of simulated multi-wavelength PA images were generated. The concentration ratio of 1:2:3:4 between the discs in each column, as well as the tenfold ratio between copper and nickel chloride were kept constant for all data sets, while the absolute concentrations of copper chloride, nickel chloride and ink were varied in three different ways:

Case I consists of 14 data sets, where the concentrations inside the discs were increased such that the average absorption coefficient of all discs increased from 0.052mm^{-1} to 0.701mm^{-1} at 810nm in equal steps. The ink concentration was kept constant for all data sets such that the total absorption coefficient of the background was 0.013mm^{-1} at 810nm. The absorption coefficients of the ink and water are shown in Fig. 2(b).

Case II consists of 13 data sets, where the concentration of the ink was increased such that the absorption coefficient of the background region at 810nm was increased from 0.003mm^{-1} to 0.258mm^{-1} in equal steps. The concentrations inside the discs were kept constant such that the average absorption of the discs was 0.252mm^{-1} at 810nm.

Case III aims to investigate the impact of spatially inhomogeneous absorption in the background. A region surrounding two of the discs containing higher concentration of ink was included. The ink concentration in this region was increased such that its absorption coefficient was increased from 0.013mm^{-1} to 0.427mm^{-1} at 810nm in 14 data sets. The concentrations of copper chloride, nickel chloride and ink outside the additional region were kept constant such that the average absorption was 0.252mm^{-1} inside the discs and 0.013mm^{-1} in the background at 810nm.

The distribution of the absorption coefficient, which is the product of the chromophore concentrations and the specific absorption coefficient, was calculated for 18 equally spaced wavelengths between 750nm and 1090nm for each data set. The scattering coefficient is zero inside the discs and between 0.728mm^{-1} and 1.067mm^{-1}

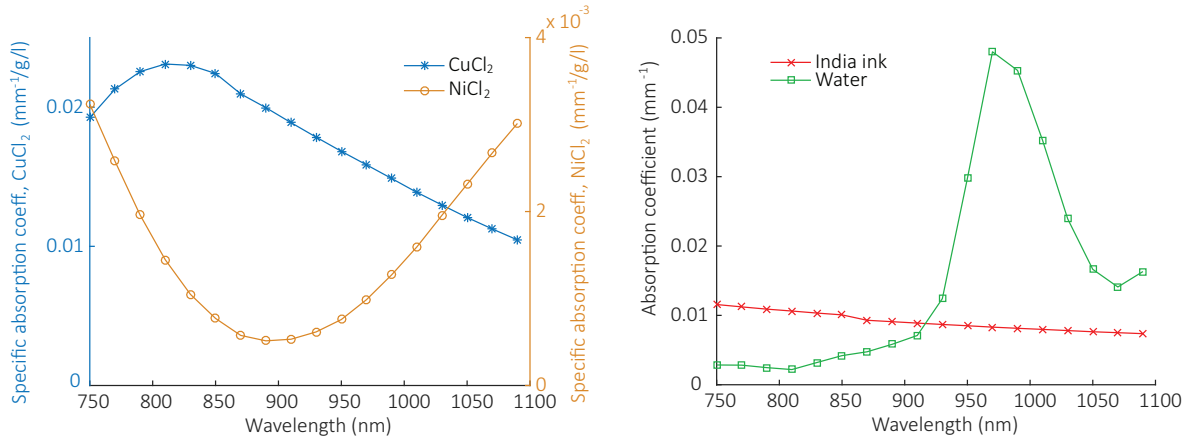

Figure 2. (a) The specific absorption coefficient of copper chloride (blue) is approximately one order of magnitude larger than that of nickel chloride (orange). (b) The green curve shows the absorption spectrum of water which was used in all data sets. The red curve shows the absorption spectrum of India ink (black) used for all data sets in Case I and III. In Case II, the absorption of ink was changed by multiplying the absorption spectrum by an constant representing the concentration. The absorption spectra of copper chloride, nickel chloride and India ink are based on spectrophotometer measurements (Lambda 750S, Perkin Elmer), and the absorption spectra of water was published by Kou *et al.*[4]

in the background depending on wavelength for all data sets. Based on the distribution of the absorption and scattering coefficients, the fluence $\mathbf{\Phi}$ was modelled using the diffusion approximation of the radiative transfer equation with the MATLAB software package TOAST++[5] for a 10mm wide line light source at the top of the phantom. The initial pressure was found by multiplying the fluence by the optical absorption coefficient and the Grüneisen parameter. The Grüneisen parameter for copper and nickel chloride is given by

$$\Gamma_i(\mathbf{r}) = \Gamma_{H_2O}(1 + \beta_i c_i), \qquad i = \text{ CuCl}_2 \text{ or NiCl}_2 \tag{5}$$

where the β_i coefficients are 5.80×10^{-3}l/g and 2.25×10^{-3}l/g for copper or nickel chloride respectively,[6] c_i denotes the concentrations of copper and nickel chloride, and Γ_{H_2O} is the Grüneisen parameter of water, which is 0.12l/g at 22°C.[7]

The forward PA wave propagation from the initial pressure distribution was modelled using the MATLAB toolbox k-Wave[8] based on a k-space pseudospectral method. The time varying photoacoustic pressure was recorded at the bottom of the numerical phantom. Images of the initial pressures were reconstructed using the time-reversal method, which back-propagates the recorded time series of the photoacoustic pressure waves. Fig. 3 shows the reconstructed images at 810nm and 1090nm for the fourth data set of each of the three Cases described above.

4. UNMIXING USING ICA AND LINEAR INVERSION

An approximate fluence adjustment was performed by dividing the simulated reconstructions of the initial pressure by an estimation of the fluence $\mathbf{\Phi}'$. The estimation of the fluence was calculated based on the simplifying assumptions that the medium is homogeneous and illuminated by an infinitely wide plane wave, such that the one dimensional solution to the diffusion approximation can be applied: $\Phi'(z,\lambda) = \Phi'_0 \exp(-\mu_{eff}(\lambda)z)$, where z is the depth from the illuminated surface, Φ'_0 is the fluence at the illuminated surface, which is assumed to be constant, μ_{eff} is the effective absorption coefficient given by $\mu_{eff} = \sqrt{3\mu_a(\mu_a + \mu'_s)}$, and μ_a and μ'_s denote the absorption and reduced scattering coefficients respectively, which in this study are assumed to be known and equal to that of the background region. This simple fluence adjustment can be applied straightforwardly in practice for *in vivo* PA images, with μ_{eff} estimated as an average parameter for the tissue.

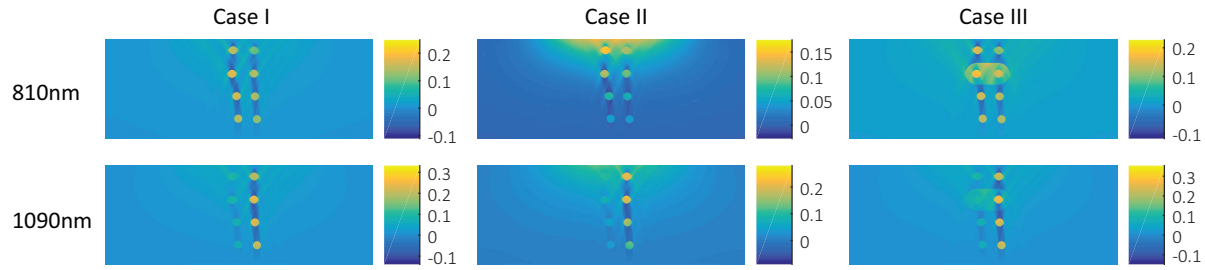

Figure 3. The reconstructions of the initial pressure for the fourth data set in each of the three Cases at 810nm (top row), where copper chloride has its absorption peak, and 1090nm (bottom row), where nickel chloride is highly absorbing. The background is more absorbing in Case II compared to Case I, and the additional region of higher ink concentration in Case III is strongly absorbing compared to the background.

The FastICA algorithm requires further pre-processing of the multi-wavelength fluence adjusted images before unmixing. The images are mean-subtracted and whitened, and principle component analysis (PCA) is used to reduce the dimensions of the image data such that only the three principle components with the largest eigenvalues of the covariance matrix of $\mathbf{P}'$ are unmixed with FastICA. Since the ordering of the estimated independent components is arbitrary, the output components are identified to the corresponding chromophores by comparing the columns in the estimated mixing matrix with the known absorption spectra of the chromophores of interest.

For comparison, the fluence adjusted images were also unmixed using LI, based on the known specific absorption spectra of copper chloride, nickel chloride, India ink and water.

4.1 Accuracy as a function of the level of absorption

The unmixed components of the fourth data set in Case I where the discs have an average absorption of 0.202mm^{-1} at 810nm are shown in Fig. 4 as an example of a case where ICA achieves higher accuracy than LI. The first column shows the components corresponding to the concentrations of copper chloride and nickel chloride separated using ICA or LI. Since ICA does not estimate the variance of each component, the magnitude of the concentration of a chromophore cannot be compared to that of another chromophore. Therefore, all components are normalised to the mean value at the disc with the highest concentration of the relevant chromophore.

The second column in Fig. 4 shows the expected components, which are the true concentration of the relevant chromophore multiplied by the Grüneisen parameter. The third column shows the error maps which represent the absolute differences between the normalised unmixed components and the expected components. The error maps are used to define three types of errors which provide a quantitative assessment of the accuracy of the unmixing methods. The concentration error, δ_c, is defined as the average error at the pixels in the discs where the chromophore of interest is present. The average error in the discs where the relevant chromophore is absent is defined as the "false positive" error, δ_f. For Case III, the false positive error also includes the error at the additional region with higher ink concentration. Lastly, the background error, δ_b, is the average error outside the eight discs.

The three types of errors as functions of the absorption coefficients in the three Cases are shown in Fig. 5. The fact that at least one type of error associated with LI is >20% for the data sets in all Cases, with the exception of the data sets where the average absorption inside the discs is very low ($<0.102\text{mm}^{-1}$ at 810nm) in Case I, demonstrates that LI is unlikely to accurately separate the chromophores.

ICA, on the other hand, is shown to achieve accurate unmixing of the chromophore concentrations with all types of errors being <10% in Case I for the data sets where the average absorption in the discs is $<0.402\text{mm}^{-1}$ at 810nm. This absorption level is comparable to that of blood, which is 0.463mm^{-1} at 810nm[9] (assuming a total haemoglobin concentration of 150g/l and 100% oxygenation). In Case II, ICA results in the concentration error being <10% provided that the background absorption is $<0.088\text{mm}^{-1}$ at 810nm, and the false positive and background errors are <20% if the background absorption is $<0.195\text{mm}^{-1}$ at 810nm. These thresholds are significantly higher than the absorption coefficient of the most common types of biological tissue, which is typically $<0.01\text{mm}^{-1}$ at 810nm.[10]

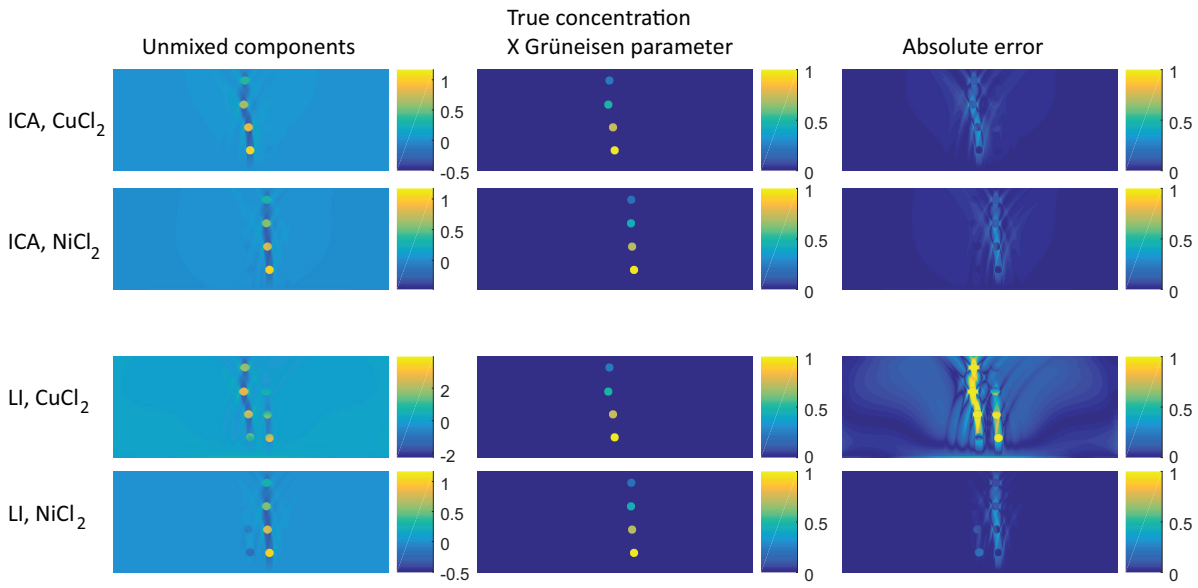

Figure 4. The results of the unmixing of the fourth data set in Case I, which has an average absorption of 0.202mm^{-1} in the discs, and 0.013mm^{-1} in the background region (at 810nm). The components corresponding to copper chloride or nickel chloride shown in the first column are more accurately separated by ICA compared to LI. The second column shows the expected components. The error maps in the third column show the absolute differences between the unmixed components and the expected components.

These results suggest that when the absorption is relatively low and hence giving rise to only moderate discrepancies between the estimated and the true fluence, components with maximal mutual independence are more likely to correspond to the true concentrations than those found with LI using the fixed absorption spectra.

However, the error trends for Case I and II also show that, at the threshold levels of absorption, the performance of ICA abruptly deteriorates. Beyond these thresholds, the accuracy of the fluence estimation is sufficiently low to lead to non-linearities so severe that the independent components found by ICA cannot be correctly identified to the relevant chromophores based on the estimated absorption spectra, hence resulting in a significant increase in errors.

The performance of both ICA and LI is ultimately dependent on the accuracy of the fluence adjustment, which in this study is determined by the level of spatial inhomogeneity in the optical properties of the phantom. This is highlighted by the fact that both methods fail to produce accurate results in the presence of the additional region with higher ink concentration in Case III. Despite this being an extreme situation where the chromophores of interest are surrounded by the additional absorber, it illustrates that the general applicability of linear methods relying on fluence adjustment is limited.

4.2 Sensitivity to fluence adjustment

In practice, the absorption of the background tissue may not be known precisely, hence giving rise to another source of inaccuracy for the fluence adjustment. The fourth data set in Case I, which has an average absorption of 0.202mm^{-1} in the discs at 810nm, was used to investigate the effect of this error. The fluence estimations for this data set were calculated using an absorption coefficient based on an ink concentration c'_{ink} that differed from the true ink concentration c_{ink} in the background region.

The errors associated with unmixing the PA images adjusted with fluence estimations based on erroneous background absorption are shown in Fig. 6. The errors associated with ICA change by less than 10% for a large range of over- and underestimation of the background absorption. This suggests that the accurate unmixing achieved by ICA at lower levels of absorption does not require knowledge of the background absorption coefficient to high precision. LI, on the other hand, is sensitive to changes in the estimation of the background

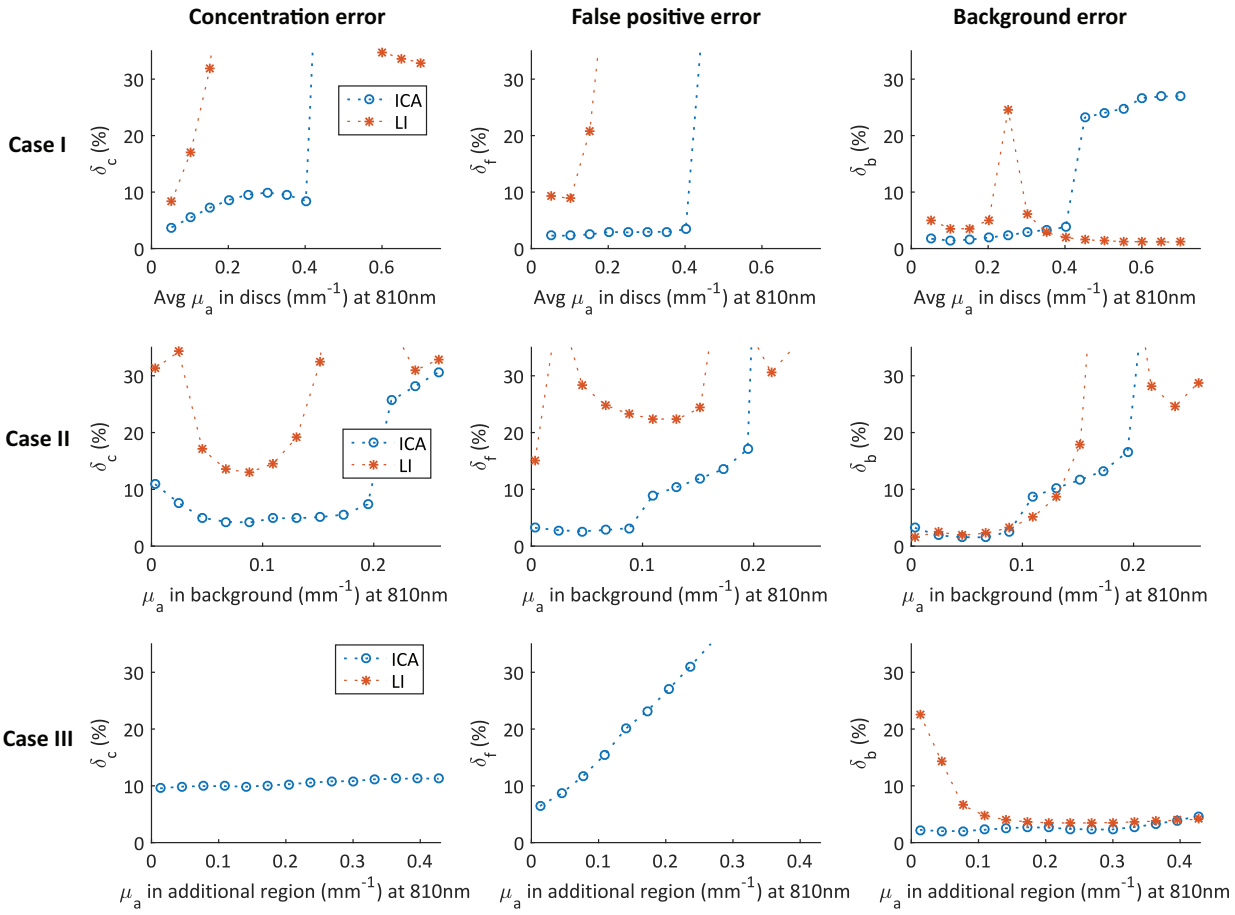

Figure 5. The concentration error (first colum), the false positive error (second column) and the background error (third column) plotted against the average absorption in the discs in Case I (first row), the absorption in the background region in Case II (second row) and the absorption in the additional region with higher ink concentration in Case III (third row). The δ_c and δ_f errors associated with LI in Case III are larger than 35% and therefore not visible within the scale of the plot.

absorption used for fluence adjustment, which is shown by the large variation in error as a function of over- and underestimation of c_{ink}.

5. DISCUSSION AND SUMMARY

Unmixing methods based on linear models have the advantages of being simple and computationally inexpensive, but the fact that they rely on using approximate models of the fluence to adjust for the non-linear spectral colouring limits their general applicability.

This study demonstrates that accurate unmixing of the chromophores can be achieved using ICA, provided that an approximate fluence adjustment has been applied and the absorption coefficients are lower than certain thresholds as well as being close to spatially homogeneous. It was shown that using the same fluence adjustment, ICA results in significantly smaller unmixing errors compared to LI for the lower ranges of absorption levels. When the absorption is higher than the thresholds, leading to greater differences between the estimated and the true fluence, the errors of ICA were shown to abruptly increase as the output components corresponding to the chromophores of interest could not be identified. These findings suggest that ICA should be used with caution, since the thresholds beyond which ICA results in large errors will vary depending on the absorption spectra, the spatial structure of the chromophores and the accuracy of the fluence adjustment.

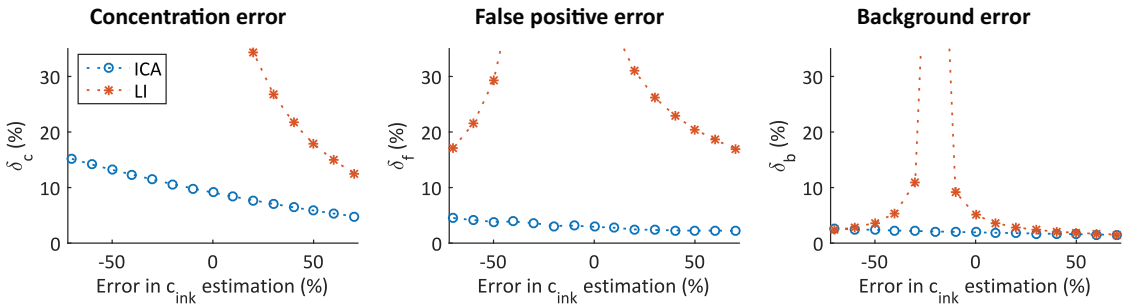

Figure 6. The errors associated with ICA and LI as a function of the difference between the concentration of the ink used for the fluence estimation and the true ink concentration in the background solution.

Another significant limitation of ICA is that it is fundamentally based on the assumption that the spatial distributions of the chromophore concentrations must be mutually independent. This assumption is valid for the chromophores in the numerical phantom used in this study, and in applications such as unmixing exogenous contrast agents from the tissue in the background. However, the independence criterion is not always fulfilled for tissue chromophores. For example, ICA cannot be used to estimate the blood oxygenation because the spatial distributions of oxy- and deoxyhaemoglobin are not independent of each other.

While ICA can under certain circumstances separate the contribution from individual chromophores, it does not provide a complete solution to the general quantitative problem in PA imaging, because it cannot estimate the absolute the chromophore concentrations. However, it may potentially be incorporated in other quantitative PA imaging methods, and used as a first step to provide information on the location and distribution of the chromophores that can be used to guide the quantification.

ACKNOWLEDGMENTS

The authors would like to thank Paul Beard for helpful discussions and acknowledge funding support from the UCL EPSRC Centre for Doctoral Training in Medical Imaging.

REFERENCES

[1] Hochuli, R., Beard, P. C., and Cox, B., "Accuracy of approximate inversion schemes in quantitative photoacoustic imaging," *Proc. SPIE* **8943**, 89435V–10 (2014).

[2] Glatz, J., Deliolanis, N. C., Buehler, A., Razansky, D., and Ntziachristos, V., "Blind source unmixing in multi-spectral optoacoustic tomography," *Opt. Express* **19**(4), 3175–3184 (2011).

[3] Hyvärinen, A. and Oja, E., "Independent component analysis: algorithms and applications," *Neural Netw.* **13**, 411–430 (2000).

[4] Kou, L., Labrie, D., and Chylek, P., "Refractive indices of water and ice in the 0.65-to 2.5-μm spectral range," *Appl. Opt.* **32**(19), 3531–3540 (1993).

[5] Schweiger, M. and Arridge, S., "The Toast++ software suite for forward and inverse modeling in optical tomography," *J. Biomed. Opt.* **19**, 040801 (2014).

[6] Laufer, J., Zhang, E., and Beard, P., "Evaluation of absorbing chromophores used in tissue phantoms for quantitative photoacoustic spectroscopy and imaging," *IEEE J. Sel. Top. Quantum Electron.* **16**(3), 600–607 (2010).

[7] Splinter, R. and Parigger, C. G., "Fluid-dynamic phenomena in cardiovascular ablation with laser irradiation," in [*Lasers in Cardiovascular Interventions*], Topaz, O., ed., 15–30, Springer London (2015).

[8] Treeby, B. E. and Cox, B. T., "k-Wave: MATLAB toolbox for the simulation and reconstruction of photoacoustic wave fields," *J. Biomed. Opt.* **15**, 021314 (2010).

[9] Prahl, S., "Optical Absorption of Hemoglobin." Oregon Medical Laser Center, http://omlc.org/spectra/hemoglobin/summary.html. (Accessed: 10 January 2016).

[10] Jacques, S. L., "Optical properties of biological tissues: a review," *Phys. Med. Biol.* **58**, R37–R61 (2013).